Chapter 33: In-Cylinder Spray, Mixing, Combustion, and Pollutant-Formation Processes in Conventional and Low-Temperature-Combustion Diesel Engines

Diesel engine performance and pollutant emissions are a result of the chemical and physical processes of the fuel jets in the combustion chamber. Important in-cylinder processes include the spatial and temporal development of liquid-fuel sprays, fuel vaporization, mixing of vaporized fuel with in-cylinder gases, low-temperature autoignition chemistry of fuel components, high-temperature chemical kinetics of combustion and pollutant formation, and late-cycle mixing and burnout processes. This chapter provides an overview of in-cylinder diesel chemical and physical phenomena, based on observations from optical diagnostic techniques of the previous chapter. Two broad categories of diesel combustion are described. The first category is conventional direct-injection diesel combustion, which is characteristic of late 20th century production diesel engines. The second category is diesel low-temperature combustion (LTC), which encompasses a wide variety of non-conventional operational strategies designed to reduce pollutant emissions in 21st century engines.

Conventional Diesel Combustion

The in-cylinder processes that affect combustion and pollutant formation in late 20th century diesel engines can vary widely across the whole map of operating conditions and engine geometries of conventional diesel combustion. Consequently, a single picture or "conceptual model" of conventional diesel combustion cannot completely describe all diesel combustion processes in all engines under all conditions. Indeed, it is far beyond the scope of this chapter to attempt to do so. However, conventional diesel jets in most engine geometries and operating maps share three general.

1. Significant Quasi-Steady Period. The first distinguishing characteristic is that the combustion event temporally overlaps with much of the fuel injection event. Fuel injection typically begins shortly before top-dead center (TDC) of the piston's stroke, when the in-cylinder gases are hot and dense. As a result, the ignition delay is short. After a subsequent premixed combustion phase, the characteristic features of the jet do not change significantly while fuel injection continues. Accordingly, the jets can be characterized as "quasi-steady." During this quasi-steady period, combustion is "mixing controlled"—chemical reaction rates of combustion are faster than the local mixing rate, so that the heat-release rate is limited primarily by mixing of vaporized fuel with in-

cylinder gases. This "typical" mode of diesel combustion ranges from moderate- to high-load conditions. Low-load conditions have short injection durations that usually yield little or no quasi-steady combustion.

2. Free Jets. Early in the fuel-injection event, diesel jets propagate relatively freely into the combustion chamber as they entrain in-cylinder gases. This "free jet" period lasts until the jet interacts with in-cylinder surfaces or flows. The duration of the free-jet period therefore depends on engine geometry (e.g., piston bowl shape and size) and operating conditions (e.g., swirl level). Large-bore engines, whose combustion chambers are typically quiescent, generally have a longer free-jet period and less flow and wall interaction than higher swirl small-bore engines. Even in a small bore engines, however, much of the initial jet development is similar to a free jet. Furthermore, although in-cylinder surfaces and flows can deflect and interact with diesel jets, the general evolution of mixing and combustion is strongly influenced by free-jet processes. Therefore, to provide a simplified framework that is independent of variations in engine geometry and in-cylinder flows, the diesel jets described in this chapter are treated as free jets.

3. Single Fuel Injection. Multiple fuel injections per cycle, including pilot, post, and split-main injections, can be beneficial for engine noise, efficiency, emissions, and management of exhaust aftertreatment devices. While these strategies can be advantageous in some conventional diesel engines, the additional complexities associated with interactions between multiple fuel injection events are not described here – only single fuel injections per engine cycle are considered.

Several conceptual models have been proposed for conventional quasi-steady diesel combustion [1-6]. The following sub-sections summarize important physical and chemical processes occurring in free diesel jets, based in part on the conceptual model of Dec [1]. The discussion begins with the initial jet development, proceeds through autoignition and premixed burning, into the quasi-steady period, and concludes with late-cycle burnout of a single conventional diesel fuel injection event.

Initial Jet Penetration

In a direct-injection diesel engine, liquid fuel is sprayed directly into the combustion chamber at high pressure through multiple orifices in the fuel injector tip. The density and pressure of the liquid fuel are each typically 20-40 times greater than the in-cylinder gases at the time of injection, near TDC. The in-cylinder jet penetration, entrainment, and mixing during most of the injection event are driven by the high-momentum of the jet.

Jet penetration may be measured by various optical techniques, including light attenuation [7,8] and elastic scattering [8-12] for non-vaporizing sprays, or by shadowgraphy and Schlieren techniques [11,13-17] and laser-induced fluorescence [18,19] for either non-vaporizing or vaporizing sprays. The penetration rate is effectively governed by exchange of momentum between the high-velocity jet and the relatively stagnant in-cylinder gases. Building on previous works including [20], Naber and Siebers [13] used a simple transient control-volume analysis assuming uniform composition, density, and velocity over the jet cross-section to derive an analytical solution for the velocity at the tip of the jet:

$$U = \frac{dx}{dt} = \frac{U_0}{2} \cdot \frac{A_0}{A(x)} \cdot \frac{\rho_f}{\rho_a} \cdot \left[\sqrt{1 + 4 \frac{A(x)}{A_0} \cdot \frac{\rho_a}{\rho_f}} - 1 \right] \tag{1}$$

Equation 1 shows that the jet tip velocity U, which is the derivative of the downstream jet penetration x with respect to time t, depends on the jet velocity at the orifice U_0, the ratio of the fuel density ρ_f to the ambient gas density ρ_a, and the ratio of the effective orifice area A_0 to the adjusted jet cross-sectional area A. (In the development of Eq. 1 [13], A was adjusted to 66% of the measured value to compensate for the uniform cross-sectional velocity assumption, so that the model penetration prediction matches measured data.) Naber and Siebers integrated a non-dimensional form of Eq. 1 yield an analytical expression for the penetration *time* as a function of *distance* (an inverse relationship), provided that U_0 is constant. Figure 1 shows the predicted penetration from Eq. 1, plotted against the non-dimensional space and time coordinates (left and bottom axes, respectively), along with experimentally measured penetration data from high-speed Schlieren photography [13]. As shown in Fig. 1, experimental penetration measurements from a wide range of conditions collapse well onto the non-dimensional analytical solution to Eq. 1.

Importantly, the analytical solution of Eq. 1 also predicts the cross-sectionally averaged equivalence ratio $\bar{\phi}$ in the quasi-steady jet, as a function of the stoichiometric fuel-to-ambient mass ratio $(F/A)_{stoich}$:

$$\bar{\phi}(x) = \frac{(F/A)_{stoich}}{\sqrt{1 + 16 \frac{A(x)}{A_0} \cdot \frac{\rho_a}{\rho_f}} - 1} \tag{2}$$

The solution to Eq. 2 is also plotted in Fig. 1, for mixing with pure air (no exhaust-gas recirculation). Equation 2 predicts that $\bar{\phi}$ varies approximately inversely with increasing

distance from the injector as more ambient gas is entrained into the jet, which is similar to both theory and experiments in fully steady jets [21]. As will be shown in the following sections, the variation of $\bar{\phi}$ along the jet axis is critically important to the evolution of many conventional diesel jet processes. Note that for many LTC jets, much of combustion occurs after the end of injection where the $\bar{\phi}$ behavior is much different than predicted by Eq. 2, as will be shown in the second half of the chapter.

Fuel Vaporization and Liquid Length

In addition to becoming less fuel-rich, mixtures farther downstream in the jet have greater sensible thermal energy due to entrainment of hot ambient gases. As a result, the jet temperature increases downstream, and the liquid fuel increasingly vaporizes. The cooling effect of fuel vaporization is balanced by the thermal energy of the entrained gases as the local liquid-vapor phase equilibrium shifts toward more vapor at greater

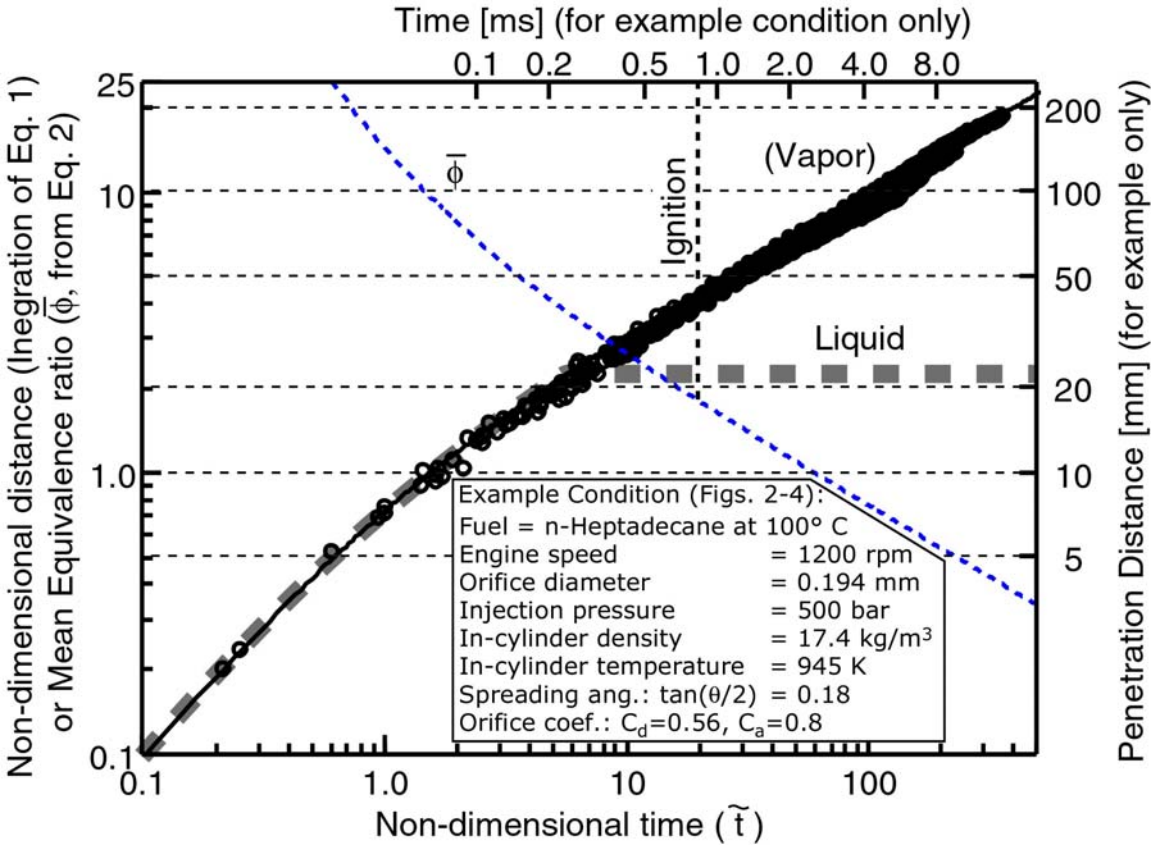

Figure 1. Measured (circles) and predicted (solid line, integration of Eq. 1) diesel-jet penetration, and predicted cross-sectionally averaged equivalence ratio (thin dotted line, Eq. 2). Left and bottom axes: non-dimensional penetration S and time $\tilde{t}$. Right and top axes: dimensional penetration and time for a single condition as listed on the figure (corresponds to images in Figs. 2-4), including predicted liquid-fuel penetration (thick dashed line).

downstream distances. During the initial penetration of a diesel jet, the local thermodynamic conditions favor a mixture of both liquid and vapor fuel, and the tip of the liquid fuel spray penetration increases with time. At some downstream distance, the thermal energy in the jet is sufficient to overcome the total latent vaporization energy of the liquid fuel, so that all of the fuel (locally) enters the vapor state. The downstream distance where the local thermodynamic conditions reach the saturated vapor state and the last bit of liquid fuel survives in the diesel jet is termed the "liquid length."

The penetration of liquid fuel may be measured from images of Mie-scattering of light off the liquid-fuel spray [8-12,22,24]. Shown on the left in Fig. 2 are a series of liquid fuel Mie-scatter images for a typical naturally aspirated operating condition [22]. The view is through a large piston-crown window. The injector is on the left, at the center of the spray pattern, and the curved line on the right indicates the location of the piston bowl-wall. The specifications for the operating condition are listed in the inset of Fig. 1, for which the right and top axes show the dimensional penetration for this condition only, using n-heptadecane fuel (a representative diesel fuel surrogate [13]). The left column of images in Fig. 2 show that the liquid-fuel penetration initially increases with time. Indeed, measurements of both liquid- and vapor-fuel penetration show that the liquid fuel initially penetrates equally with the overall jet [16,18,19,25], as illustrated by the initial overlap of the liquid- and vapor-fuel penetration in Fig. 1. Then, at some time after the start of injection (ASI), the liquid penetration reaches a quasi-steady value, which is the

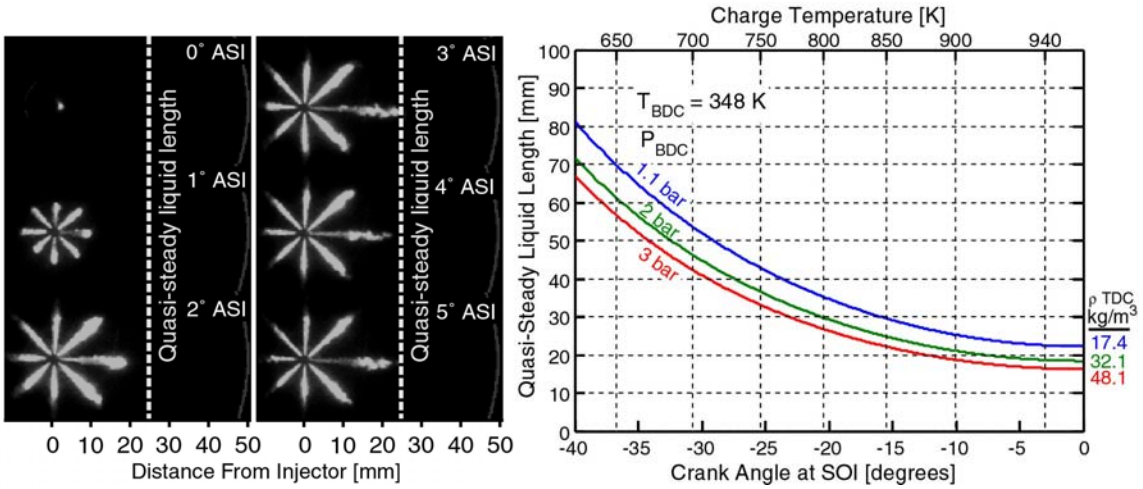

Figure 2. Left: Mie-scatter images of liquid fuel from a heavy-duty diesel engine [22] at same conditions as Figs. 3 and 4, and as inset in Fig. 1. Right: Quasi-steady liquid-fuel penetration predicted by Siebers' scaling correlation [23] for diesel fuel as the in-cylinder temperature and density change during compression/expansion for three different boost levels at constant BDC temperature.

liquid length. The right column of images in Fig. 2 also illustrate that by 3° (crank angle) ASI, or 0.42 ms at 1200 rotations per minute (rpm), the liquid-fuel penetration length remains nearly constant – the quasi-steady liquid length (vertical dotted line) is established. Note that as illustrated in Fig. 1, the vapor jet continues to penetrate after the liquid fuel reaches its quasi-steady liquid length.

Accurate prediction of the quasi-steady liquid length is important because of the potential for liquid-fuel impingement on in-cylinder surfaces, which can inhibit mixing, increase emissions, and cause oil-dilution problems. Using Eqs. 1 and 2, along with detailed thermodynamic state data for fuel and entrained gases, Siebers derived a scaling law to predict the quasi-steady liquid length (L) [23]:

$$L = \frac{b}{a} \cdot \sqrt{\frac{\rho_f}{\rho_a}} \cdot \frac{\sqrt{C_a} \cdot d}{\tan(\theta/2)} \sqrt{\left(\frac{2}{B} + 1\right)^2 - 1} \tag{3}$$

In Eq. 3, b and a are correlation constants with suggested values of 0.41 and 0.66, respectively, C_a is the orifice area contraction coefficient, d is the orifice diameter, θ is the jet spreading full angle, and B is the mass ratio of fuel to ambient gas at the liquid length, i.e., where the enthalpy change in the ambient gases matches the energy required to heat and vaporize the liquid fuel at the local liquid-vapor equilibrium temperature. The predictions of Eq. 3 agree well with laser-elastic Mie scattering measurements of the liquid length over a wide range of conditions. The success of Eq. 3 in predicting the liquid length, along with its independence of injection pressure, implies that for modern high-pressure diesel sprays, fuel vaporization is controlled by mixing, rather than atomization processes [23].

Shown on the right side in Fig. 2 is the dependence of the predicted liquid length on the engine crank angle for a typical heavy-duty injector and operating conditions, including several intake boost levels. The liquid length decreases as TDC is approached because the in-cylinder gases become hotter and more dense, so that the jet penetrates shorter distances before sufficient thermal energy is entrained to vaporize the fuel. For conventional naturally aspirated diesel operating conditions with near-TDC injection, the liquid length is approximately 25 mm, which is well short of distances to in-cylinder surfaces in large-bore engines. Hence, diesel fuel sprays in conventional large-bore engines do not experience liquid wall impingement at typical, warmed-up operating conditions. Fuel injectors in small-bore engines typically have smaller nozzle offices, which give a shorter liquid length (Eq. 3), though some liquid impingement may still occur.

Importantly, the plot on the right side of Fig. 2 shows that intake pressure boosting can reduce the liquid length by increasing the density of the entrained gases. Figure 2 also shows that if fuel injection occurs away from TDC, when the in-cylinder gases are cooler and less dense, the liquid fuel penetration is greater. Thus, the potential for liquid-fuel impingement on in-cylinder surfaces increases with early or late injection, though increasing boost still helps to shorten the liquid length. This behavior has implications for the LTC conditions that are described in the second half of this chapter.

Autoignition and Premixed Burning

Diesel fuels typically display two-stage ignition chemistry [26]. At lower temperatures (800-1000 K), the first-stage of ignition forms a pool of hydrogen peroxide (H_2O_2). After the first-stage of ignition, the H_2O_2 pool builds as the temperature rises to approximately 1200 K, where it breaks down to release hydroxyl (OH) during the hotter second-stage ignition and premixed burn. Typical heat-release rate analysis (derived from measured cylinder pressure), however, usually does not show a distinct separation between first- and second-stage ignition for conventional diesel combustion due to the rapid rise in temperature. First- and second-stage ignition are apparent, however, in optical data.

Optical diagnostics show that autoignition in conventional diesel combustion typically occurs when much of the jet is still fuel-rich. That is, the jet penetration is relatively short at the time of ignition, so the cross-sectionally averaged equivalence ratios, as predicted by Eq. 2, are fuel-rich, even at the head of the jet. The spatial location of ignition can be detected using chemiluminescence imaging [27], laser-induced fluorescence [1], or Rayleigh-scattering [28]. Figure 3 shows chemiluminescence images from the same engine and similar conditions as the liquid-fuel images in Fig. 2. Near 4° (0.56 ms) ASI, the ignition chemiluminescence is first detectable from 10 to 30 mm downstream of the injector. Equation 2 (also see Fig. 1) predicts mean equivalence ratios in the range from 3 to 10 in this region.

By 6° ASI, the strong second-stage chemiluminescence is between 20 and 40 mm downstream, where Eq. 2 predicts mean equivalence ratios from 2 to 4. Rayleigh-scattering measurements confirm that the equivalence ratios at second-stage ignition are indeed in the range of 2-4 [28]. Furthermore, the same Rayleigh scattering measurements show that at ignition, fuel molecules are consumed nearly simultaneously throughout the jet cross-section, over a wide range of stoichiometric to fuel-rich mixtures, unlike classic flame propagation [28]. The premixed burn increases the temperature in jet, and the

resulting hot, partially oxidized mixtures synthesize PAH soot precursors that go on to form soot.

Quasi-Steady Period

The period after ignition and premixed burning through to the end of injection is the quasi-steady period, during which significant soot is formed in the hot, fuel-rich core of the jet. A layer of OH forms along the periphery of the jet during the premixed burn, and remains throughout the quasi-steady period. The OH layer at the interface between the fuel-rich jet and the surrounding oxidizing gases indicates that the mixing-controlled combustion occurs largely in a diffusion, or non-premixed, flame.

Evidence of soot formation within the jet can be provided by several optical techniques [29], including natural soot luminosity imaging, spectroscopic analysis such as the two-color technique, light extinction, and planar laser-induced incandescence (PLII). The location of the diffusion flame may be observed from PLIF images of OH,

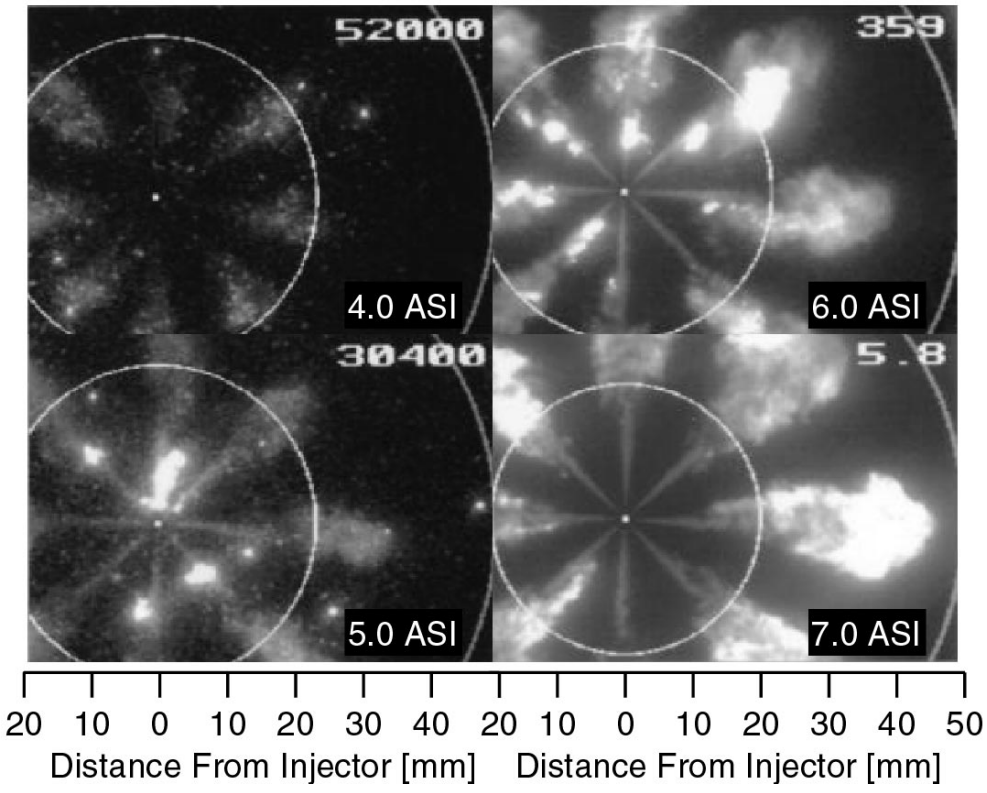

Figure 3. Chemiluminescence images of diesel autoignition for the same conditions as Figs. 2 and 4, and as listed in Fig. 1 (images taken from [27]). The small dot on the middle-left is the injector, the large circle shows the quasi-steady liquid length (see images in Fig. 2), and the white arc on the right is the piston bowl-wall. The number in the top left corner is the relative camera gain.

which is formed in hot diffusion flames [30]. Simultaneous images of soot PLII and OH-PLIF are shown in Fig. 4 at various times after the start of injection for a condition similar to Figs. 2, and 3 [31]. Unlike Figs. 2 and 3, however, the view for the images in Fig. 4 is through a window in the cylinder head (see figure caption).

Both the soot and the OH typically first appear near the peak heat-release rate of the premixed burn (6° or 0.84 ms ASI). The soot appears and remains throughout the fuel-rich cross-section of the jet as it continues to penetrate during the quasi-steady period. The green OH-PLIF images show that a thin layer of OH surrounds the jet, at the boundary between the fuel-rich jet and the surrounding ambient gases. In typical flames, OH concentrations are greatest in regions of intermediate stoichiometries, in the neighborhood of ϕ=1 [32]. The OH therefore marks the location of a relatively thin stoichiometric diffusion flame on the jet periphery, which suggests steep fuel concentration gradients on the jet periphery. Indeed, Rayleigh-scattering images show steep equivalence ratio gradients on the periphery of the jet [28].

Typically, neither the soot nor the diffusion flame extend upstream all of the way to the

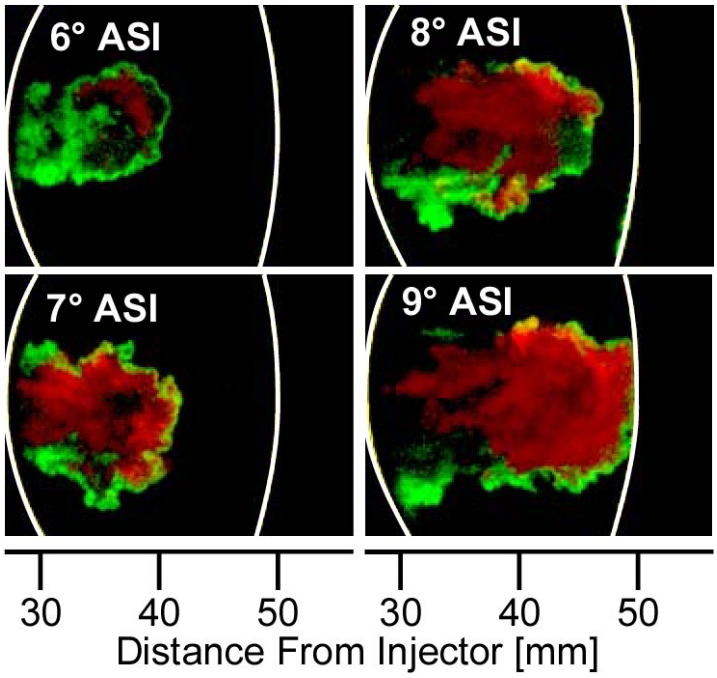

Figure 4. Simultaneous images of OH-PLIF (green) and soot-PLII (red) for conditions similar to Figs. 2 and 3 (images taken from [31]). The curved white line on the left is the edge of the cylinder-head window, and the curved white line on the right is the piston bowl-wall. The injector is to the left of the images, outside of the field of view, as indicated by the scale below the images.

injector. Rather, the diffusion flame stands off from the injector a finite distance, termed the "lift-off length" [33]. The soot resides throughout the jet cross-section within the envelope of the diffusion flame, somewhat downstream of the lift-off length. This description of a soot-filled jet surrounded by a diffusion flame continues throughout the quasi-steady period, until the end of fuel injection.

Soot formation within the jet depends on the local equivalence ratio and temperature in the jet. To illustrate the dependence of soot formation on equivalence ratio and temperature in diesel jets, Kitamura et al. [34], Kamimoto and Bae [36], Akihama et al. [37], and others plotted contours of soot formation over a range of equivalence ratio and temperature. An example of a chemical kinetics simulation for soot yield adapted from Kitamura et al. [34] is shown in Fig 5. The soot yields in Fig. 5 were calculated for a residence time of 2 ms with temperature, pressure, and equivalence ratio held constant. Fig. 5 predicts that soot forms at in-cylinder conditions within a peninsula bounded by temperature limits near 1500 and 2600 K, and a lower equivalence ratio limit of ϕ=2.

Hypothetical ϕ–T paths of mixing and combustion for diesel jets are also shown on the left plot of Fig. 5, both for conventional in-cylinder gases with 21% O_2 (red) and highly diluted gases with 8% O_2 (blue). Prior to ignition, most mixtures in the jet are above the ϕ=2 lower equivalence ratio limit for soot formation. However, prior to ignition, the temperature in the jet (<1000 K) is too low for soot formation (i.e., mixtures are outside

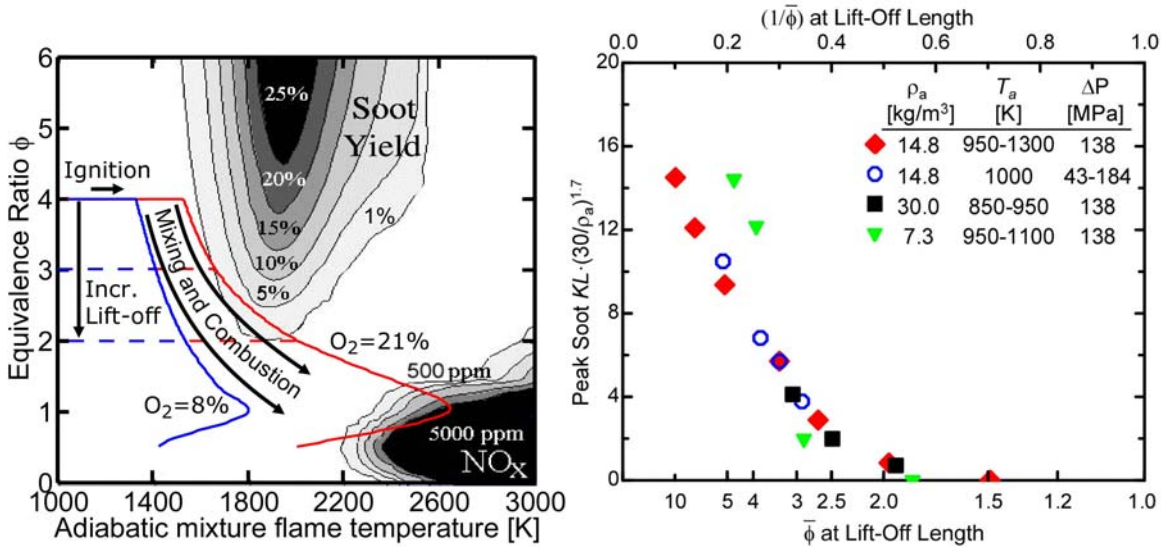

Figure 5. Left: Soot and NOx formation in ϕ–T coordinates, adapted from Kitamura et al. [34]. The red blue lines show the diesel jet mixing and combustion pathways for 21% and 8% ambient gas oxygen concentration, respectively. Right: Dependence of in-cylinder soot on the equivalence ratio at the flame lift-off length [35].

of the plot in Fig. 5, to the left). After ignition, the premixed burn raises the temperature, as depicted by the horizontal portion of the diesel-jet paths in Fig. 5. After ignition, the timescale for combustion reactions is typically much shorter than the mixing time, so that the hypothetical ϕ–T curve follows a mixing-limited path, at the local flame temperature.

Soot forms in conventional diesel combustion (red curve) as the mixtures approach the 1% soot-formation threshold. Then, as the jet continues to penetrate, the mixtures follow a path deeper into the soot peninsula in Fig. 5, leading to formation of more soot during the quasi-steady period. (The blue curve for LTC conditions will be discussed in later sections of this chapter.)

The soot typically forms somewhat downstream of the lift-off length [6]. The continued formation of soot after the premixed burn indirectly indicates that during the quasi-steady period, the temperature within the jet must be above the soot formation threshold (approx. 1500 K, Fig. 5). Dec hypothesized that oxygen entrained into the jet upstream of the lift-off length would partially oxidize the fuel in a rich, partially-premixed reaction zone downstream of both the liquid length and the lift-off length [1]. Furthermore, entrainment and mixing of hot products from the diffusion flame into the center of the jet also increases the temperature of the fuel-rich, soot-producing core of the jet. Both the premixed reaction zone and the entrainment of hot products that lead to soot formation occur downstream of the lift-off length. Therefore, the high-temperature diffusion flame lift-off length controls the downstream distance where temperatures are high enough for subsequent soot formation in diesel jets. But, as shown in Fig. 5, soot formation also depends on ϕ, which is also controlled by the lift-off length. As shown in Fig. 1 and according to Eq. 2, the jet cross-sectionally averaged equivalence ratio decreases with downstream distance. As shown in the ϕ–T plot of Fig. 5, with increasing lift-off length, the diesel jet mixing path avoids more of the soot-formation peninsula. Optical measurements confirm that soot formation decreases with decreasing equivalence ratio at the lift-off length. The graph on the right side in Fig. 5 shows the soot optical density, measured by laser extinction [35], plotted versus the jet cross-sectionally averaged equivalence ratio (from Eq. 3) at the diffusion flame lift-off length, measured by OH chemiluminescence imaging [38]. In Fig. 5, soot decreases with the equivalence ratio at the lift-off length, reaching essentially zero soot for $\overline{\phi}$ <2, consistent with the ϕ–T concept shown on the left in Fig. 5. When $\overline{\phi}$ >2, the soot varies approximately linearly with $1/\overline{\phi}$ (top axis in Fig. 5).

While the diffusion flame lift-off length is clearly important for soot formation in the jet, the conditions necessary to completely inhibit soot formation by achieving $\overline{\phi}$ <2 at the

lift-off length are extreme compared to conventional diesel combustion. Such conditions require extremely small nozzle orifices, very long ignition delays (low cetane fuels or cool conditions), or very high injection pressures [39]. Furthermore, the rate of soot oxidation, as well as soot formation, affects the ultimate exhaust soot emissions. Some of the factors that increase the diffusion flame lift-off length, such as decreasing ambient temperature, also tend to decrease soot oxidation. As a result, exhaust soot may increase even as the soot formation decreases at longer lift-off lengths because soot oxidation decreases more rapidly than soot formation [40].

The diffusion flame is also important for the other primary pollutant from conventional diesel engines, nitrogen oxides (NOx). In diesel engines, exhaust NOx has been shown to vary strongly with the adiabatic flame temperature over a wide range of conditions [41,42], indicating that the thermal NO formation route is dominant over other potential mechanisms (e.g., the prompt NO or the N_2O pathways). The strong temperature dependence means that NO formation should be strongly weighted to regions with the highest temperature, such as the stoichiometric diffusion flame. Figure 5 shows that NO formation increases rapidly as the diesel jet mixtures approach high temperatures up to 2600 K, in the bottom right corner of the ϕ–T plot where ϕ<2. Indeed, planar laser-induced fluorescence imaging of NO shows that the NO initially forms in the diffusion flame, where temperatures are highest [43]. A contrary observation is the correlation of exhaust NOx with the size of the premixed burn, which suggests that the premixed burn is responsible for NOx formation. However, the optical data show that the premixed burn of conventional diesel combustion is too rich to form significant NOx, so other factors must be responsible for the correlation. By contrast, large portions of LTC jets with long ignition delays are closer to stoichiometric, so that a larger fraction of the total NOx may be formed during the premixed burn, as will be shown later in this chapter

Late-Cycle Burnout

The quasi-steady period ends with the end of fuel injection, after which the apparent heat-release rate decreases as the remaining fuel, combustion intermediate species, and soot continue to oxidize as they mix with in-cylinder gases. Although the heat-release rate is low compared to the quasi-steady period, oxidation reactions can persist late into the expansion stroke, as evidenced by fluorescence images of strongly oxidizing OH surrounding soot imaged by LII, even after exhaust-valve opening under some conditions [44]. Indeed, the diffusive combustion zone structure of the quasi-steady jet is generally maintained, with OH residing on the perimeter and between the soot pockets.

Late in the cycle, the initial large pockets of soot formed by each of the diesel jets break down into smaller pockets, with ever broadening distributions of OH between the pockets. Soot-LII [44] and combustion luminosity measurements [45] show that the persistence of soot very late into the cycle, even after exhaust valve opening, changes significantly with fuel injection timing and duration (i.e., engine load). Combined soot-LII and OH-PLIF imaging [44] shows that soot in the quasi-steady diesel jet may survive into the exhaust gases by two mechanisms. First, if fuel injection is retarded, the time available before exhaust valve opening may be insufficient to complete the oxidation of the soot. Second, if the piston contents cool sufficiently during the expansion stroke to quench the oxidation reactions (i.e., OH is no longer present), soot may survive into the exhaust stroke. This second mechanism typically occurs because of dilution with exhaust-gas recirculation (EGR), and may occur even at modest EGR rates (~10%) [44].

Positive Ignition-Dwell Low-Temperature Diesel Combustion

As described in the previous section, the mixing and combustion processes of quasi-steady jets in conventional diesel combustion create a hot (>1500 K), fuel-rich, soot-forming core surrounded by an even hotter (~2600 K) NO-forming diffusion flame on the periphery of the jet. Diesel low-temperature combustion (LTC) strategies generally seek to reduce combustion temperatures and/or increase pre-combustion mixing to avoid both the fuel-rich soot formation regions and the high-temperature NO-formation zone. For example, EGR dilution can shift the ϕ–T mixing and combustion path to the left from the red curve (21% O_2) toward the blue curve (8% O_2) in Fig. 5. (The 8%-O_2 example will be discussed in more detail later in the chapter.) As a result, the mixing and combustion processes of low-temperature diesel jets create a much different picture of in-cylinder pollutant formation. A wide variety of engine and fuel delivery concepts have been pursued to achieve these basic goals of LTC. A complete treatment of the whole gamut of reported LTC concepts is beyond the scope of this chapter. Instead, two important subsets of diesel LTC that are currently used in many production early 21st century diesel engines will be described. Both of these LTC subsets share the following common three important characteristics:

1. Conventional Diesel Fuel-Injection Hardware. Fuel delivery and mixing is critical to the performance of low-temperature diesel engines, and a variety of non-conventional diesel fuel-delivery strategies have been reported, including premixing outside the combustion chamber, as in many homogeneous-charge compression ignition (HCCI) concepts [46], narrow-angle direct injection [47,48], and impinging jets [49,50]. The mixing processes and jet geometries for these strategies are so different from those of conventional diesel direct injection systems that they preclude a side-by-side comparison with conventional diesel combustion described in the first half of this chapter. Diesel LTC can also be implemented, however, using conventional diesel fuel injection hardware, by injecting fuel either early or late in the cycle to provide extended time for the premixing required to inhibit soot formation. The LTC concept considered here features conventional diesel multi-hole direct-injection systems having a standard, wide included angle between jets.

2. Low-Temperature Combustion by EGR Dilution. The low flame temperatures necessary to reduce NOx can be achieved either by burning locally fuel-lean throughout the combustion chamber, as in fully premixed HCCI engines [46], or by diluting the

intake charge with exhaust-gas recirculation (EGR) [51]. While the fuel-lean, fully premixed HCCI approach is promising, it is difficult to create a fully premixed charge for HCCI with conventional diesel fuel-injection hardware. Moreover, the relatively homogeneous in-cylinder mixtures required for HCCI bear little resemblance to the heterogeneous jet structures of conventional diesel combustion. Instead, EGR-diluted LTC, which is used in many current production diesel LTC concepts, is the focus of discussion in this chapter.

3. Single Fuel Injection. As with conventional diesel combustion, many diesel LTC concepts use multiple fuel injections per cycle to affect the in-cylinder distribution of fuel beyond what can be achieved with a single injection. Many different concepts have been proposed, and it is beyond the scope of this chapter to describe the in-cylinder processes for multiple injections. Instead, the descriptions of diesel low-temperature combustion are restricted to single fuel-injection events.

With the above characteristics in common, the two LTC subsets differ in whether or not the jets experience significant quasi-steady combustion. The first subset discussed below is for LTC strategies with positive ignition dwell, where ignition occurs after the end of injection. These conditions are typically low-load conditions that do not have a quasi-steady period. The chapter concludes with description of the second subset, quasi-steady LTC, which applies to higher loads, where fuel injection continues after ignition.

Fuel Vaporization and Liquid Length

Soot formation may be reduced either by increasing the amount of premixing of fuel with the intake charge prior to autoignition and combustion, or by reducing the combustion temperatures. Increased premixing moves the mixtures that react during the premixed burn downward from the soot formation peninsula in Fig. 5 into lower equivalence ratios, similar to the effect of increasing lift-off length described for conventional diesel combustion. Increased dilution, such as by EGR, moves the combustion temperatures leftward from the soot peninsula, as shown by the blue curve in Fig. 5.

The mixing time is extended by increasing the ignition delay. Intake charge dilution by cooled EGR extends the ignition delay to provide more time for mixing prior to combustion. Indeed, studies show that with EGR dilution, the ignition delay is approximately inversely proportional to the in-cylinder oxygen concentration [52,53]. However, the increase in ignition delay with EGR, and the accompanying increase in mixing time prior to combustion, is offset by the lower ambient oxygen concentrations, for which longer mixing times are required to reach a given equivalence ratio.

Another way to increase the ignition delay is to inject fuel when the in-cylinder gases are cooler, so that ignition reactions are slower. As shown in Fig. 2, the in-cylinder charge temperature decreases when fuel injection occurs farther from TDC, so the ignition delay can be extended by either injecting early [54-58] or late [59-61] in the cycle. With fuel injection away from TDC, however, the liquid fuel penetration tends to increase, as shown in Fig. 2. Depending on engine geometry, as the injection timing is advanced or retarded from TDC, liquid fuel may impinge on the piston or cylinder wall, causing poor mixing and emissions problems from liquid films [48,62,63] or lubrication oil dilution [50,64,65]. Figure 2 shows that boosting the intake to higher pressures can help to reduce the liquid fuel penetration.

In many LTC strategies, both intake charge dilution and early or late fuel injection are combined to increase mixing prior to combustion. An example of liquid fuel penetration and ignition chemiluminescence for a low-boost, early-injection LTC condition using dilution is shown in Fig. 6, which is taken from Singh et al. [66]. Fuel injection starts at

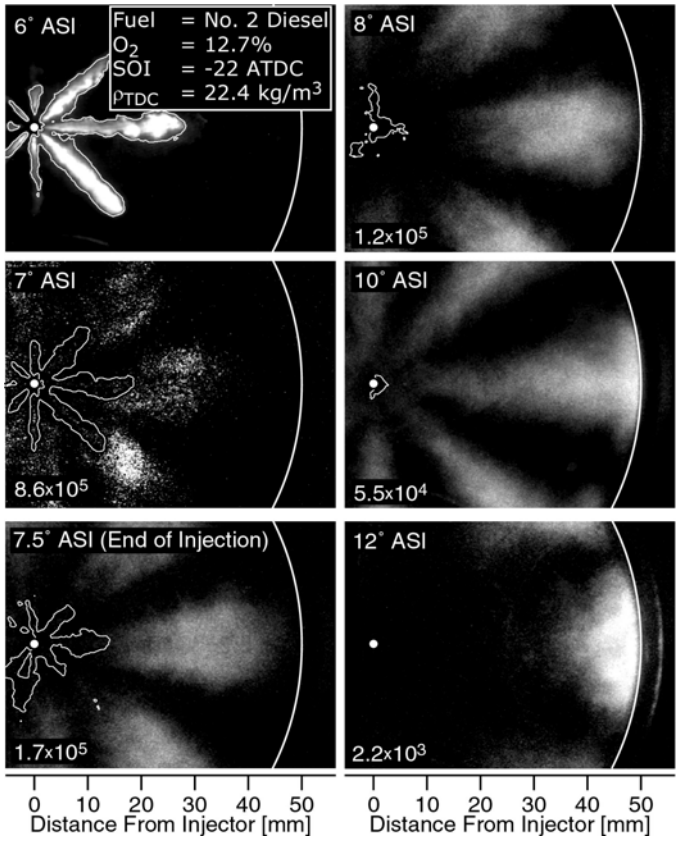

Figure 6. Simultaneous images of liquid fuel contours and ignition chemiluminescence (grayscale) for a low-load early-injection LTC condition of Singh et al. [66] (see inset). The camera gain is given on the bottom left of the images.

-22° ATDC and ends near 7.5° ASI. The intake oxygen concentration is 12.7% (equivalent to 50-60% EGR), and the intake pressure is slightly boosted (22.4 kg/m^3 in-cylinder density at TDC). The top-left image in Fig. 6 shows the liquid-fuel Mie-scattering at 6° ASI, with a contour marking the outer edge at 15% of maximum intensity. For all other images in Fig. 6, the chemiluminescence is displayed in grayscale, and the outer contour of the liquid fuel is overlaid for comparison. (Chemiluminescence imaging will be described in the next section).

The initial evolution of the liquid-fuel penetration (not shown here) is very similar to that of conventional diesel combustion (Fig. 2). Although the ambient density increases slightly during the injection event, the quasi-steady liquid-length reaches a relatively constant value of approximately 30 mm from 4° to 6° ASI. The liquid length typically varies from cycle to cycle [22], in this case reaching nearly 40 mm on some cycles. Thus, for this particular low-boost condition, the liquid fuel always vaporizes before reaching in-cylinder surfaces (piston bowl radius is 50 mm in this heavy-duty engine). However, for a similar condition with lower intake-pressure boost (giving 16 kg/m^3 TDC density, rather than 22.4 kg/m^3), some liquid fuel reaches the piston bowl wall (50 mm from injector) on some engine cycles [32]. Even then, however, the modest energy release from first-stage ignition reactions can raise temperatures in the jet to assist fuel vaporization [32]. Indeed, in Fig. 6, the liquid length begins to decrease after 6° ASI, when chemiluminescence emission appears at the beginning of the first-stage ignition heat release [66]. This observation suggests that if first-stage ignition occurs at the proper time, it could help to prevent liquid-fuel impingement on in-cylinder surfaces. Even without first-stage ignition heat release, however, other data also indicate that end-of injection mixing processes may also decrease the liquid fuel penetration near the end of injection [67].

Autoignition and Premixed Burning

With longer ignition delay for diluted gases, and with fuel injection farther from TDC, into lower density gases, the diesel jet penetrates farther downstream before ignition. As a result, the autoignition reactions occur farther downstream. For the LTC operating condition in Fig. 6, the initial ignition chemiluminescence begins 20 to 40 mm downstream, near 7-7.5° ASI, compared to 15 to 25 mm downstream and 4-4.5° ASI for conventional diesel combustion (Fig. 3). Within 2-3° after its first detectable appearance at 7° ASI, first-stage ignition chemiluminescence occurs throughout the jet, nearly from the injector to the tip of the jet. The indications of ignition spanning the length of the jet

are further supported by laser-induced fluorescence images of formaldehyde, which also fills the jet after forming rapidly during the first-stage ignition [68]. Complementary equivalence ratio measurements show that the mixtures where formaldehyde initially appears span from fuel-lean to fuel rich [68]. During the second-stage ignition and premixed burning, the most intense chemiluminescence is emitted from the downstream regions of the jet, along the piston bowl-wall, as shown in Fig. 6 at 12° ASI. The considerable increase in the intensity of the chemiluminescence suggests that second-stage combustion is more intense near the bowl wall.

Indeed, a few crank angle degrees later in the cycle, near the peak of the premixed burn heat release, OH-PLIF typically first appears in the same downstream area. For example, Fig. 7 shows simultaneous OH-PLIF (green) and soot luminosity (red) images for a similar early-injection LTC condition as shown in Fig. 6, but with a lower intake boost level, giving a TDC density of 16 kg/m^3 [32]. The view in Fig. 7 is similar to Fig. 4, though in Fig. 7 a portion of the bowl-rim was removed to allow the jet to penetrate as a free jet past the nominal piston bowl-wall (dashed line) all the way to the cylinder wall (white arc on right side of images). OH marks the transition to the hot, second stage chemistry. Therefore, the appearance of OH downstream, combined with the strong ignition chemiluminescence in Fig. 6, indicates that most of the premixed-burn heat release occurs in the downstream region of the jet.

Rather than forming in a thin diffusion flame at the periphery of the jet as in conventional

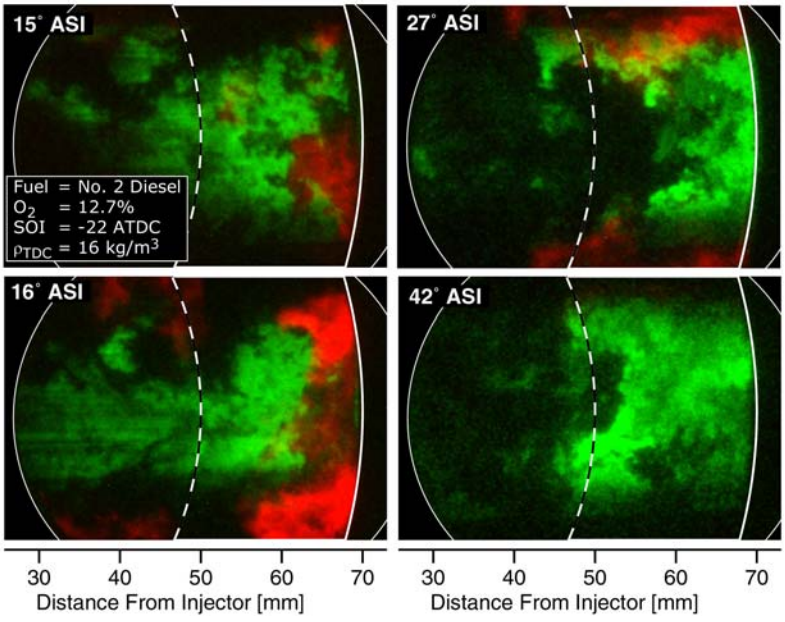

Figure 7. Simultaneous images of OH-PLIF (green) and soot-luminosity (red) for a low-boost early-injection LTC condition [32] (see inset). The curved white line on the left is the edge of the cylinder-head window, the curved dashed line is the usual location of the bowl rim, and the white arc on the right is the piston cylinder wall.

diesel combustion, the OH-PLIF appears in heterogeneous, sometimes ribbon-like structures throughout the downstream region of the jet. The OH-PLIF distribution in the downstream region broadens rapidly after its first appearance, though it still remains heterogeneous with small dark patches distributed throughout the jet cross-section. The appearance of OH in the jet cross section indicates that the jet is much leaner than a conventional diesel jet. As described in the first half of this chapter, conventional diesel jets are too fuel-rich to accumulate detectable OH in the soot-filled jet cross-section (see Fig. 4). With significant OH throughout its cross-section, much of the downstream LTC jet must be of intermediate stoichiometry, in the neighborhood of ϕ=1.

Indeed, direct measurements of the equivalence ratio in LTC jets show that mixtures very rapidly become fuel-lean after the end of injection, especially near the injector. Shown in Fig. 8 are equivalence ratio measurements in an LTC jet at 5° (0.70 ms) after the end of injection (AEI), as measured by fuel-vapor Rayleigh-scattering [69]. The ambient conditions and fuel injection parameters for Fig. 8 are similar to the engine conditions for Figs. 6 and 7, though the injector orifice diameter is smaller (0.100 mm in Fig. 8 compared to 0.196 mm in Figs. 6 and 7). The equivalence ratio contour map in Fig. 8 is a composite of two images, one showing from 2 to 25 mm from the injector, and the other showing from 25 to 60 mm from the injector. Much of the jet downstream of 30 mm, where OH appears in Fig. 7, is near ϕ=1, with even leaner mixtures (ϕ<1) closer to the injector. Equivalence ratio measurements in the engine at conditions similar to Figs. 6 and 7 show similar equivalence ratios of intermediate stoichiometry where OH appears, and with even leaner mixtures upstream [69].

The lean mixtures that form upstream in the LTC jets are certainly a consequence of the

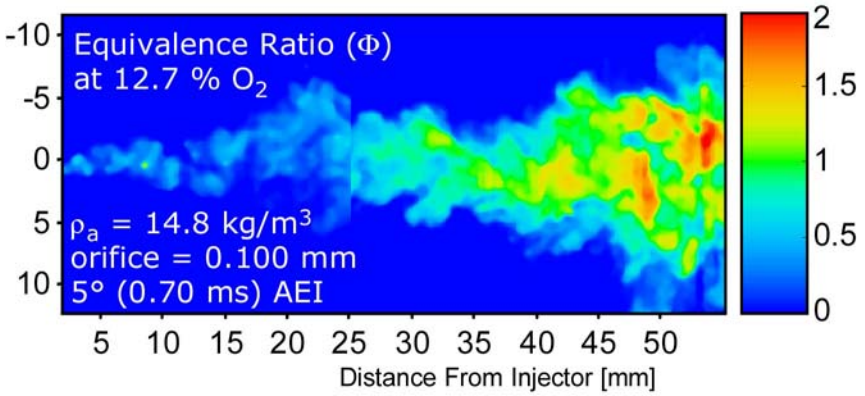

Figure 8. Composite of two Rayleigh scattering images, covering 2 to 25 mm and 25 to 60 mm from the injector, showing contour maps of equivalence ratio 5° (0.70 ms) after the end of injection (AEI) in a single jet, taken from [69].

increased premixing time of LTC combustion, but they are also surprising for two reasons. First, the intake charge for the LTC condition is diluted by EGR, so all mixtures in the jet should become richer because of the reduced oxygen concentration. That is, Fig. 1 shows that a quasi-steady jet without dilution has ϕ~3 at 30 mm, with even richer mixtures upstream. With similar dilution as in Figs. 6, 7, and 8, the equivalence ratio 30 mm downstream in Fig. 1 would be nearly ϕ=5, yet shortly after the end of injection, the LTC jet has near-unity equivalence ratios in the same region. Second, and more importantly, the LTC jet structure is very similar to that of conventional diesel combustion. That is, the jet is still roughly conical in shape, with nearly the same width. Therefore, at a given downstream location, the jet cross-sectional area, or amount of entrained ambient gases, is similar to that of conventional diesel jets. And yet, in a very short time after the end of injection, the equivalence ratio becomes much lower than in the quasi-steady jet, even with EGR, as indicated by the widespread appearance of OH in the jet cross section. Consequently, the equivalence ratio distribution shortly after the end of injection must be radically different from the approximately 1/x dependence of the equivalence ratio in Fig. 1 and Eq. 2 that applies to a steady jet. This implies that mixing processes occurring after the end of injection are significantly different than those occurring during injection—mixtures at a given downstream location rapidly become much leaner after the end of injection than they would during the injection.

Consistent with the rapidly leaning jet, and in contrast to conventional diesel combustion, very little soot appears in the jet for the LTC conditions. Furthermore, its appearance is much less repeatable than for conventional diesel combustion, with significant cycle-to-cycle variation in the exact location of the onset of soot. As a result, the location of soot in the jet can be measured more repeatably by soot luminosity imaging, as shown in Fig. 7, than by laser-induced incandescence. In general, soot does not appear throughout the mid- and downstream portions of the jet as in conventional diesel combustion, but rather only far downstream in the jet and off to the sides of the jet. The downstream region where the soot appears is roughly coincident with the “roll-up” vortex at the head of the jet, and also with the region where the jet impinges onto the cylinder wall in Fig. 7. According to the ϕ–T plot in Fig. 5, soot formation is expected only when ϕ>2. This implies that after the end of injection, the richest regions of the jet are far downstream, not upstream as in a quasi-steady jet, as shown by the direct measurements in Fig. 8.

Even late in combustion, OH-PLIF generally remains in the downstream portion of the jet, and it typically does not appear upstream. As shown in Fig. 7, late in the cycle, the OH-PLIF does not appear upstream of about 50 mm from the injector. In another study

with more optical access to the upstream jet, but with late injection, OH never appeared upstream, though strong formaldehyde fluorescence did remain upstream [70]. Chemical kinetics simulations suggest that formaldehyde formed in the main jet during the first-stage ignition would persist late in the cycle if mixtures were too lean for complete combustion, with ϕ<0.5 [70]. Indeed, Fig. 8 shows that equivalence ratios near the injector do become very low after the end of injection, which may lead to unburned hydrocarbon emissions because of incomplete combustion for conditions with long ignition delays [69].

Quasi-Steady Low-Temperature Diesel Combustion

The characterization of LTC described above applies to a variety of strategies that are typically limited to relatively low-load conditions. In general, these low-load conditions with short injection durations have significant time for mixing between the end of injection and the start of combustion, and thus lower soot emissions. High-load operating conditions, by contrast, typically may have injection durations that exceed the ignition delay, even when in-cylinder gases are diluted with EGR, and especially when injection occurs near TDC. Although significant NOx-formation is avoided by charge dilution, the quasi-steady jet may still have significant fuel-rich, soot-forming regions, similar to conventional diesel combustion. Indeed, quasi-steady LTC jets are similar in many ways to conventional quasi-steady jets, but EGR dilution changes several important characteristics of the reacting jets, as will be discussed in this section.

Initial Jet Development

With injection occurring near TDC, the fuel vaporization for quasi-steady LTC fuel jets is controlled by energy entrained with the hot, high-density gases. Therefore, a quasi-steady liquid penetration length is established, as with conventional quasi-steady jets (Fig. 2). The ignition processes of quasi-steady LTC fuel jets also follow a two-stage process as with conventional diesel combustion. However, hot, second-stage ignition is delayed because of low in-cylinder oxygen concentrations. The increased ignition delay allows more time for jet penetration and mixing prior to ignition. The initial reacting sections of the LTC jet are therefore farther from the injector compared to conventional diesel combustion [71,72], as was shown for the low-load LTC condition discussed in the previous section. However, once ignited, a structure characterized by a lifted diffusion flame surrounding a fuel-rich jet core is established [73,74], similar to conventional diesel combustion described in the early part of this chapter.

LTC Exhaust "Soot Bump"

Even though a typical diffusion flame structure is established for quasi-steady LTC, EGR dilution significantly alters the diesel combustion and pollutant-formation processes. Evidence for these changes is provided in Fig. 9, which shows exhaust smoke measurements for multiple operating conditions on the left, and NOx and UHC emissions for a range of fuels on the right, assembled from multiple studies [37,75-82]. The emissions data are plotted versus the intake oxygen mole fraction, rather than EGR rate, because the EGR rate required to yield a given intake oxygen mole fraction can vary significantly with engine load and intake pressure. However, in general, the EGR

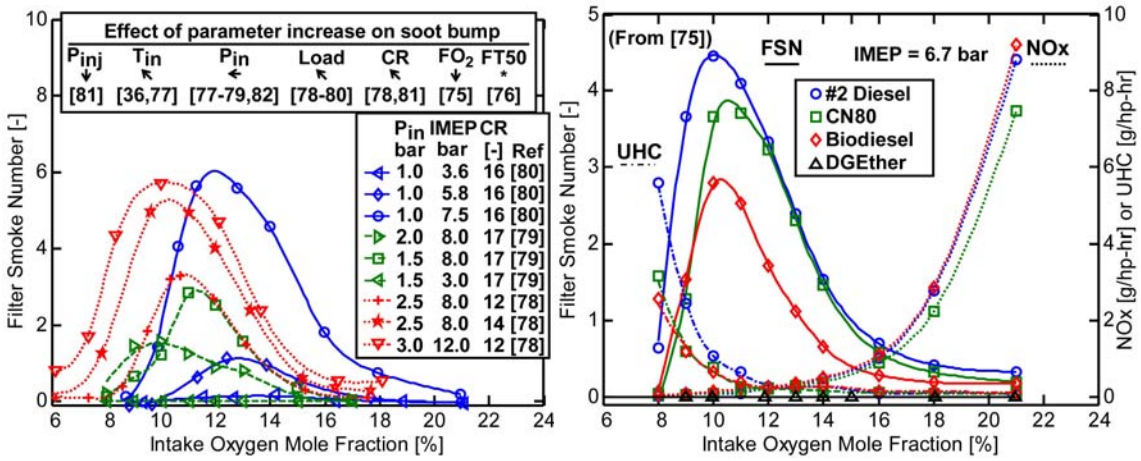

Figure 9. Left: exhaust smoke measurements for multiple operating conditions in multiple engines, assembled from references indicated on the graph. Upper legend arrow indicates how the soot bump is affected by an increase in fuel injection pressure (Pinj), intake temperature (Tin), intake pressure (Pin), compression ratio (CR), fuel oxygen mass percent (FO_2), or fuel 50% boiling point temperature (FT50), based on the cited references below the arrow. Right: Exhaust smoke, NOx, and UHC emissions for a range of fuels, taken from [75].

percentage increases, and the exhaust excess oxygen decreases, with decreasing intake oxygen mole fraction. The intake pressure (P_{in}), engine load (IMEP, indicated mean-effective pressure), compression ratio (CR), and literature references are provided on the figure to distinguish each operating condition. Because of fundamental differences between engine facilities, the absolute magnitudes of the emissions should be compared using results from the same facility only.

Beginning with no EGR (21% O_2), an initial reduction in intake oxygen mole fraction reduces NOx emissions, but increases smoke emissions. The EGR reduces diesel combustion flame temperatures, thereby reducing NOx emissions, but the lower oxygen concentration and combustion temperature can lead to incomplete oxidation of soot and an increase in exhaust smoke. This behavior is an example of the classic trade-off between NOx and particulate matter (PM) emissions. However, with further reduction in intake oxygen, the emission measurements show that exhaust smoke reaches a maximum somewhere between 10-13% oxygen and then decreases to almost zero near 6-8% oxygen. This maximum in exhaust smoke with decreasing intake oxygen percent has been referred to as the soot "bump" [78,79,82]. The existence of the soot bump, which indicates a decline of PM and NOx emissions with decreasing intake oxygen concentration, is interesting to LTC because it represents behavior that is contrary to the classic PM-NOx tradeoff.

Seeking to mitigate exhaust PM at quasi-steady LTC conditions, researchers have investigated the response of the soot bump over a wide range of engine operating conditions. Their findings are summarized in the upper left inset in Fig. 9, with an arrow indicating the change in magnitude and direction of the soot bump with respect to intake oxygen concentration for a given parameter. For example, an increase in engine load corresponds to an arrow pointing up and to the left, which indicates an increase in the soot bump, and a shift of the peak in the soot bump to lower oxygen mole fraction. Note that low-load conditions, with an IMEP of 4 bar or less, which include the LTC experimental conditions discussed with Figs. 6-7, produce little PM emissions. Moderate- to high-load conditions, with higher IMEP and more quasi-steady LTC, generally have higher PM emissions. However, low PM emissions remain a possibility at high-load, provided the intake oxygen concentration is below the level at the peak of the soot bump.

LTC In-Cylinder "Soot Bump"

By themselves, exhaust PM measurements provide limited information about the effects of EGR on soot formation within the reacting diesel fuel spray. For example, *exhaust* PM levels may increase with increasing EGR because of less effective soot oxidation, even as peak in-cylinder soot levels decrease because of reduced soot formation. To better understand soot formation, in-cylinder soot levels can be directly measured by optical diagnostics, including laser extinction. Shown in Fig. 10 are in-cylinder laser-extinction soot volume fraction measurements from quasi-steady, mixing-controlled diesel fuel jets in a constant-volume vessel, for oxygen concentrations ranging from 21% to 8% [83]. Soot volume fraction (f_v) contours are shown in the left of Fig. 10 for five different EGR levels for an experimental condition with an ambient temperature of 1000 K and an ambient density of 14.8 kg/m^3 (42 bar). The quasi-steady lift-off lengths are shown as dashed vertical lines, along with estimates of $\overline{\phi}$ for each lift-off length *(H)*, from Eq. 2.

As shown in Fig. 10, left, the quasi-steady lift-off length increases with EGR, but the equivalence ratios at the lift-off length are virtually constant [73,74,83]. In other words, the lift-off length increases to compensate for decreasing in-cylinder oxygen concentration, thereby producing similar fuel-oxygen mixtures at the quasi-steady lift-off length. A similar compensating effect applies to the mixture composition at the time of ignition. For a jet at ignition, EGR increases the ignition delay and the time for mixing prior to reaction, but the reduction in oxygen concentration by EGR offsets the increased

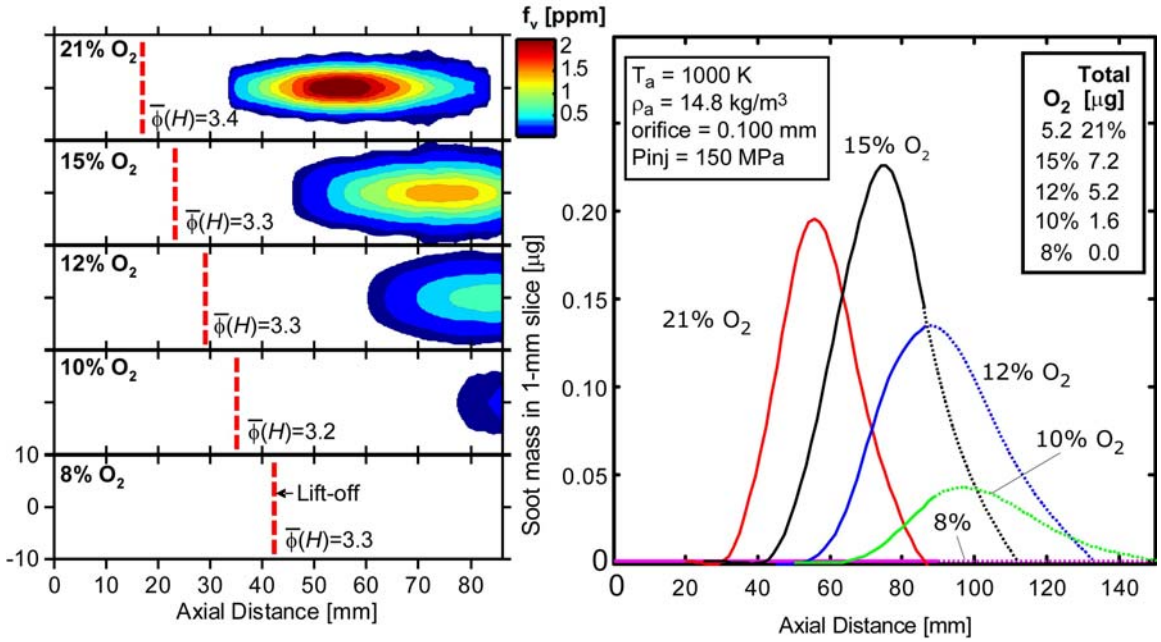

Figure 10. In-cylinder laser-extinction soot volume fraction measurements from quasi-steady, mixing-controlled diesel fuel jets in a constant-volume vessel, for oxygen concentrations ranging from 21% to 8% at the conditions listed in the inset [83]. Left: soot volume fraction contours, with equivalence ratios noted at the lift-off lengths (vertical dashed lines). Right: integrated soot mass in 1-mm slices, derived from contours on left.

mixing time. Consequently, the equivalence ratio at ignition remains approximately constant [71]. The net result is that the stoichiometry of incipient soot-forming mixtures in the central core of the jet remains approximately the same while in-cylinder oxygen concentration is decreased.

The colorbar of Fig. 10 shows that the peak f_v decreases substantially with decreasing oxygen concentration, in agreement with [83]. The soot formation and soot oxidation regions also move farther downstream from the injector. When the oxygen volume fraction is decreased to 8%, it appears that the sooting region of the jet may have been pushed beyond the field of view. However, further experiments using both laser-induced incandescence of soot near the back wall of the vessel and luminosity imaging of the entire vessel show that no soot formation is detectable anywhere in the vessel at the 8%-O_2 condition [83].

Although the peak f_v decreases with increasing EGR, more important questions are whether the total mass of soot increases or decreases, and whether or not soot formed within the reacting jet escapes oxidation and becomes PM. For example, the 21%-O_2 fuel

jet appears to have efficient oxidation of soot formed upstream, such that little (if any) soot escapes oxidation at the downstream tip of the flame. To quantify the total mass of soot within the jet as a function of axial distance, the f_v data were integrated over the cross-section of the jet [83]. Soot mass at each axial position is shown for 1-mm "slices" at the right of Fig. 10. For a given in-cylinder oxygen concentration, the soot mass at first increases, then reaches a peak, and finally decreases with increasing axial distance. With decreasing ambient oxygen, the peak soot mass in the axial profile increases to a maximum at 15% O_2 and then decreases to zero at 8% O_2. Note that the soot mass is higher at 15% O_2 compared to 21% O_2, even though the peak f_v is lower, because the sooting region of the jet is wider (greater volume). As a result, the integrated mass is higher despite the generally lower f_v.

These direct measurements of *in-cylinder* soot mass in quasi-steady reacting sprays therefore show that the soot "bump" occurs at 15% O_2 for these conditions (Fig. 10), compared to 10-12% O_2 for exhaust soot (Fig. 9). This difference in the location of the in-cylinder and exhaust soot bumps is largely due to differences in the extent of soot oxidation between the constant-volume chamber and an engine. In the quasi-steady reacting spray of Fig. 10, the combustion event occurs at constant volume and only a small fraction of the oxygen available in the chamber is consumed by the single, reacting fuel jet (low overall equivalence ratio). Consequently, ambient temperatures and pressures remain high, excess oxygen is available, and soot oxidation may proceed to completion as oxygen is mixed into downstream regions of the jet. In an engine, less excess oxygen is available to mix into the reacting jet because of a smaller in-cylinder volume per jet, as well as interactions between neighboring fuel jets. The time available for soot oxidation is also limited by the piston motion. During the expansion stroke, the in-cylinder contents cool, and soot oxidation reactions slow. Furthermore, as the in-cylinder oxygen concentration is reduced, flame temperatures become lower, so that soot oxidation can be more readily quenched during the expansion stroke. Therefore, expansion should shift the in-cylinder soot bump to lower oxygen concentrations where soot oxidation is quenched. Indeed, one optical engine study with significant expansion after initial soot formation [40], the exhaust soot bump was near 10% O_2, consistent with the data in Fig. 9, but the in-cylinder soot bump was near 12% O_2, compared to 15% for the constant-volume combustion chamber [83].

Analysis from [83,84] shows that the cause of the *in-cylinder* soot bump for quasi-steady jets with sufficient time for complete soot oxidation is a tradeoff between residence time in soot forming regions and the soot formation rates within those regions. The residence

time increases with decreasing in-cylinder oxygen concentration because more in-cylinder gas must be mixed into the jet to reach a given equivalence ratio to complete combustion, requiring additional time to accomplish this mixing. On the other hand, decreasing in-cylinder oxygen concentration reduces combustion temperatures, which slows the rate of soot formation. The tradeoff between an increased residence *time* and a reduced *rate* of soot formation essentially determines the in-cylinder oxygen concentration for which the peak in-cylinder soot accumulation is maximum. At high ambient oxygen concentration, a high temperature promotes fast soot formation but rapid oxygen entrainment then quickly impedes soot formation and oxidizes the soot. For very low oxygen concentrations (8% O_2), the soot formation rate is so low that soot does not form despite long residence times. This is illustrated on the ϕ–T diagram of Fig. 5, where the 8%-O_2 curve (blue) shows that the mixing and reaction path of the jet occurs at temperatures far to the left of the soot peninsula, and thus too low for soot formation [37,39].

While the in-cylinder soot bump occurs at 15% O_2 for the conditions of Fig. 10, variation in the in-cylinder pressure or temperature causes the soot bump to shift to different in-cylinder oxygen concentrations, because of temperature and pressure effects on soot formation and oxidation. Increases in temperature and pressure are known to significantly increase soot formation rates in lifted diesel flames [35,83]. This change to the soot formation rate creates a different tradeoff between oxygen concentration effects on residence time and the increased rate of soot formation, as well as many of the exhaust soot-bump trends depicted in Fig. 9. For example, increases in compression ratio, engine load, or intake temperature, result in higher in-cylinder gas temperatures. The increased gas temperature, coupled with higher residence time at low oxygen concentration, causes more soot formation in fuel jets at lower in-cylinder oxygen concentration, thereby shifting the soot bump to lower in-cylinder oxygen concentration [83]. Once again, this shift in *in-cylinder* soot formation is consistent with exhaust soot trends for the soot bump shown in Fig. 9.

Closing Remarks on LTC Diesel Research Needs

Current optical diagnostic data have revealed that LTC-jet in-cylinder processes, which are responsible for the performance and emissions of LTC strategies, are significantly different than those of conventional diesel jets. Accordingly, the current understanding of conventional diesel combustion must be extended and updated to include LTC operating conditions, thereby aiding the development of LTC strategies. The existing

conceptual models for conventional diesel combustion have proven very useful, not only as foundations of understanding, but also as springboards for research and development concepts and bases for computer modeling efforts. Extensions of these conceptual models to LTC conditions will promote further development and refinement of LTC strategies. As described in this chapter, many aspects of in-cylinder LTC phenomena have been revealed by optical diagnostic techniques, but further research is still required to fill in missing details needed for the model extensions.

One critical need for further research is improved understanding of mixing processes that occur during the ignition dwell between the end of injection and the start of combustion. Mixture preparation occurring during the ignition dwell, prior to combustion, is critical to the subsequent ignition, combustion, and pollutant formation processes of LTC engines. Although some of the important "symptoms" of mixing during the ignition dwell have been revealed, the underlying fluid mechanical causes for rapid mixing occurring after the end of injection are not well understood. Another need is for better understanding of post-combustion mixing, including its effects on both formation and oxidation of soot, especially late in the engine cycle. Existing conceptual models describe much of the quasi-steady period of diesel jets, but late-cycle mixing processes have not been explored in as much detail. The reduced soot oxidation rates of diluted, LTC strategies emphasize the importance of late-cycle mixing and soot oxidation, especially at higher loads. Finally, various multiple-injection concepts have demonstrated significant improvements in performance and exhaust emissions for LTC engines. The role of interactions between multiple injections in mixture preparation prior to combustion, as well as in post-combustion mixing, has not been adequately explored by optical diagnostics. Additional insights into the important in-cylinder mechanisms of multiple-injection operating conditions are needed to support further conceptual model extensions to multiple injections for both conventional and LTC diesel combustion.

Reference List

1. Dec, J. E., "A Conceptual Model of D.I. Diesel Combustion Based on Laser-Sheet Imaging," SAE Paper 970873, SAE Transactions, **106**, No. 3, pp. 1319-1348, 1997.

2. Bruneaux, G., "A Study of Soot Cloud Structure In High Pressure Single Hole Common Rail Diesel Injection Using Multi-Layered Laser-Induced Incandescence," Comodia 2001, Nagoya, Japan, 2001.

3. Taschek, M., Koch, P., Egermann, J., and Leipertz, A., "Simultaneous Optical Diagnostics of HSDI Diesel Combustion Processes," SAE Paper 2005-01-3845, 2005.

4. Kosaka, H., Aizawa, T., and Kamimoto, T., "Two-Dimensional Imaging of Ignition and Soot Formation Processes in a Diesel Flame," Int.J.Engine Res., **6**, No. 1, pp. 21-42, 2005.

5. Idicheria, C. A. and Pickett, L. M., "Formaldehyde Visualization Near Lift-Off Location in a Diesel Jet," SAE Paper 2006-01-3434, SAE Transactions, **115**, No. 4, pp. 683-695, 2006.

6. Pickett, L. M. and Siebers, D. L., "Soot Formation in Diesel Fuel Jets Near the Lift-Off Length," Int.J.Engine Res., **6**, pp. 103-130, 2006.

7. Hiroyasu, H. and Arai, M., "Structures of Fuel Sprays in Diesel Engines," SAE Paper 900475, SAE Transactions, **99**, No. 3, pp. 1050-1061, 1990.

8. Coghe, A., Araneo, L., Brunello, G., and Cossali, G. E., "Experimental Investigation of Gas Density Effects on Diesel Spray Penetration and Entrainment," SAE Paper 1999-01-0525, SAE Transactions, **108**, No. 3, pp. 679-693, 1999.

9. Arrègle, J., Pastor, J. V., and Ruiz, S., "The Influence of Injection Parameters on Diesel Spray Characteristics," SAE Paper 1999-01-0200, 1999.

10. Gupta, S., Poola, R., and Sekar, R., "Effect of Injection Parameters on Deisel Spray Characteristics," SAE Paper 2000-01-1600, SAE Transactions, **109**, No. 3, pp. 1713-1718, 2000.

11. Bae, C., Yu, J., Kang, J., Kong, J, and Lee, K. O., "Effect of Nozzle Geometry on the Common-Rail Diesel Spray," SAE Paper 2002-01-1625, 2002.

12. Alfuso, S., Allocca, L., Auriemma, M., Caputo, G., Corcione, F. E., Montanaro, A., and Valentino, G., "Analysis of a High Pressure Diesel Spray at High Pressure and Temperature Environment Conditions," SAE Paper 2005-01-1239, 2005.

13. Naber, J. D. and Siebers, D. L., "Effects of Gas Density and Vaporization on Penetration and Dispersion of Diesel Sprays," SAE Paper 960034, SAE Transactions, **105**, No. 3, pp. 82-111, 1996.

14. Ahmadi-Befrui, B., Wiesler, B., and Winklhofer, E., "The Propagation of Fuel Sprays in a Research Diesel Engine - A Joint Numberical and Experimental Analysis," SAE Paper 910181, SAE Transactions, **100**, No. 3, pp. 209-220, 1991.

15. Su, T. F., Farrell, P. V., and Nagarajan, R. T., "Nozzle Effect on High Pressure Diesel Injection," SAE Paper 950083, SAE Transactions, **103**, No. 3, pp. 177-188, 1995.

16. Kennaird, D. A., Crua, C., Lacoste, J., Heikal, M. R., Gold, M. R., and Jackson, N. S., "In-Cylinder Penetration and Break-Up of Diesel Sprays Using a Common-Rail Injection System," SAE Paper 2002-01-1626, 2002.

17. Desantes, J. M., Payri, R., Salvador, F. J., and Soare, V., "Study of the Influence of Geometrical and Injection Parameters on Diesel Sprays Characteristics in Isothermal Conditions," SAE Paper 2005-01-0913, 2005.

18. Bergstrand, P., Persson, F., Forsth, M., and Denbratt, I., "A Study of the Influence of Nozzle Orifice Geometries on Fuel Evaporation Using Laser-Induced Exciplex Fluorescence," SAE Paper 2003-01-1836, SAE Transactions, **112**, No. 4, pp. 1264-1275, 2003.

19. Kim, T., Beckman, M. S., Farrell, P. V., and Ghandhi, J. B., "Evaporating Spray Concentration Measurements from Small and Medium Bore Diesel Injectors," SAE Paper 2002-01-0219, 2002.

20. Wakuri, Y. Fujii M., Amitani, T., and Tsuneya, R., "Studies of the Penetration of Fuel Spray in a Diesel Engine," Bulletin of JSME, **3**, No. 9, 1960.

21. Ricou, F. P. and Spalding, D. B., "Measurements of Entrainment by Axisymmetrical Turbulent Jets," J.Fluid Mech., **11**, No. 1, pp. 21-32, 1961.

22. Espey, C. and Dec, J. E., "The Effect of TDC Temperature and Density on the Liquid-Phase Fuel Penetration in a D.I. Diesel Engine," SAE Paper 952456, SAE Transactions, **104**, No. 4, pp. 1400-1416, 1995.

23. Siebers, D. L., "Scaling Liquid-Phase Fuel Penetration in Diesel Sprays Based on Mixing-Limited Vaporization," SAE Paper 1999-01-0528, SAE Transactions, **108**, No. 3, pp. 703-728, 1999.

24. Siebers, D. L., "Liquid-Phase Fuel Penetration in Diesel Sprays," SAE Paper 980809, SAE Transactions, **107**, No. 3, pp. 1205-1227, 1998.

25. Pickett, L. M. and Hoogterp, L., "Fundamental Spray and Combustion Measurements of JP-8 at Diesel Conditions," SAE Paper 2008-01-1083, 2008.

26. Westbrook, C. K., "Chemical Kinetics of Hydrocarbon Ignition in Practical Combustion Systems," Proc.Combust.Inst., **28**, pp. 1563-1577, 2000.

27. Dec, J. E. and Espey, C., "Chemiluminescence Imaging of Autoignition in a D.I. Diesel Engine," SAE Paper 982685, SAE Transactions, **107**, No. 3, pp. 2230-2254, 1998.

28. Espey, C., Dec, J. E., Litzinger, T. A., and Santavicca, D. A., "Planar Laser Rayleigh Scattering for Quantitative Vapor-Fuel Imaging in a Diesel Jet," Combust.Flame, **109**, pp. 65-86, 1997.

29. Zhao, H. and Ladommatos, N., "Optical Diagnostics for Soot and Temperature Measurement in Diesel Engines," Prog.Energy Combust.Sci., **24**, pp. 221-255, 1998.

30. Dec, J. E. and Coy, E. B., "OH Radical Imaging in a DI Diesel Engine and the Structure of the Early Diffusion Flame," SAE Paper 960831, SAE Transactions, **105**, No. 3, pp. 1127-1148, 1996.

31. Dec, J. E. and Tree, D. R., "Diffusion-Flame / Wall Interactions in a Heavy-Duty DI Diesel Engine," SAE Paper 2001-01-1295, SAE Transactions, **110**, No. 3, pp. 1618-1634, 2001.

32. Musculus, M. P. B., "Multiple Simultaneous Optical Diagnostic Imaging of Early-Injection Low-Temperature Combustion in a Heavy-Duty Diesel Engine," SAE Paper 2006-01-0079, SAE Transactions, **115**, No. 3, pp. 83-110, 2006.

33. Siebers, D. L. and Higgins, B. S., "Flame Lift-Off on Direct-Injection Diesel Sprays Under Quiescent Conditions," SAE Paper 2001-01-0530, SAE Transactions, **110**, No. 3, pp. 400-421, 2001.

34. Kitamura, T., Ito, T., Kitamura, Y., Ueda, M., Senda, J., and Fujimoto, H., "Soot Kinetic Modeling and Empirical Validation on Smokeless Diesel Combustion with Oxygenated Fuels," SAE Paper 2003-01-1789, SAE Transactions, **112**, No. 4, pp. 945-963, 2003.

35. Pickett, L. M. and Siebers, D. L., "Soot in Diesel Fuel Jets: Effects of Ambient Temperature, Ambient Density, and Injection Pressure," Combust.Flame, **138**, pp. 114-135, 2004.

36. Kamimoto, T. and Bai, X., "High Combustion Temperature for the Reduction of Particulate in Diesel Engines," SAE Paper 880423, SAE Transactions, **97**, No. 3, pp. 692-701, 1988.

37. Akihama, K., Takatori, Y., Inagaki, K., Sasaki, S., and Dean, A. M., "Mechanism of the Smokeless Rich Diesel Combustion by Reducing Temperature," SAE Paper 2001-01-0655, SAE Transactions, **110**, No. 3, pp. 648-662, 2001.

38. Higgins, B. and Siebers, D., "Measurement of the Flame Lift-Off Location on D.I. Diesel Sprays using OH Chemiluminescence," SAE Paper 2001-01-0918, SAE Transactions, **110**, No. 3, pp. 739-753, 2001.

39. Pickett, L. M. and Siebers, D. L., "Non-Sooting, Low Flame Temperature Mixing-Controlled DI Diesel Combustion," SAE Paper 2004-01-1399, SAE Transactions, **113**, No. 4, pp. 614-630, 2004.

40. Huestis, E., Erickson, P. A., and Musculus, M. P. B., "In-Cylinder and Exhaust Soot in Low-Temperature Combustion Using a Wide-Range of EGR in a Heavy-Duty Diesel Engine," SAE Paper 2007-01-4017, SAE Transactions, **116**, 2007.

41. Plee, S. L., Ahmad, T., and Myers, J. P., "Flame Temperature Correlation for the Effects of Exhaust Gas Recirculation on Diesel Particulate and NOx Emissions," SAE Paper 811195, SAE Transactions, **90**, No. 4, pp. 3738-3754, 1981.

42. Plee, S. L., Ahmad, T., Myers, J. P., and Faeth, G. M., "Diesel NOx Emissions - A Simple Correlation Technique for Intake Air Effects," Proc.Combust.Inst., **19**, pp. 1495-1502, 1982.

43. Dec, J. E. and Canaan, R. E., "PLIF Imaging of NO Formation in a DI Diesel Engine," SAE Paper 980147, SAE Transactions, **107**, No. 3, pp. 176-204, 1998.

44. Dec, J. E. and Kelly-Zion, P. L., "The Effects of Injection Timing and Diluent Addition on Late-Combustion Soot Burnout in a DI Diesel Engine Based on Simultaneous 2-D Imaging of OH and Soot," SAE Paper 2000-01-0238, 2000.

45. Upatnieks, A. and Mueller, C. J., "Investigation of the Relationship between DI Diesel Combustion Processes and Engine-Out Soot Using an Oxygenated Fuel," SAE Paper 2004-01-1400, 2004.

46. Assanis, D., Najt, P. M., Dec, J. E., Eng, J. A., Asmus, T. N., and Zhao, F., *Homogeneous Charge Compression Ignition (HCCI) Engines - Key Research and Development Issues*, SAE, Warrendale, PA, 2003.

47. Walter, B. and Gatellier, B., "Development of the High Power NADI Concept Using Dual Mode Diesel Combustion to Achieve Zero NOx and Particulate Emissions," SAE Paper 2002-01-1744, SAE Transactions, **111**, No. 4, pp. 779-787, 2002.

48. Kanda, T., Hakozaki, T., Uchimoto, T., Hatano, J., Kitayama, N., and Sono, H., "PCCI Operation with Fuel Injection Timing Set Close to TDC," SAE Paper 2006-01-0920, 2006.

49. Wahlin, F. and Cronhjort, A., "Fuel Sprays for Premixed Compression Ignited Combustion - Characteristics of Impinging Sprays," SAE Paper 2004-01-1776, 2004.

50. Akagawa, H., Miyamoto, T., Harada, A., Sasaki, S., Shimazaki, N., Hashizume, T., and Tsujimura, K., "Approaches to Solve Problems of the Premixed Lean Diesel Combustion," SAE Paper 1999-01-0183, SAE Transactions, **108**, No. 3, pp. 120-132, 1999.

51. Ladommatos, N., Abdelhalim, S. M., Zhao, H., and Hu, Z., "The Dilution, Chemical, and Thermal Effects of Exhaust Gas Recirculation on Diesel Engine Emissions - Part 1: Effect of Reducing Inlet Charge Oxygen," SAE Paper 961165, 1996.

52. Pickett, L. M., Siebers, D. L., and Idicheria, C. A., "Relationship between Ignition Processes and the Lift-Off Length of Diesel Fuel Jets," SAE Paper 2005-01-3843, SAE Transactions, **114**, No. 3, pp. 1714-1731, 2005.

53. Kook, S., Bae, C., Miles, P. C., Choi, D., and Pickett, L. M., "The Influence of Charge Dilution and Injeciton Timing on Low-Temperature Diesel Combustion and Emissions," SAE Paper 2005-01-3837, SAE Transactions, **114**, No. 4, pp. 1575-1595, 2005.

54. Takeda, Y., Keiichi, N., and Keiichi N., "Emission Characteristics of Premixed Lean Diesel Combustion with Extremely Early Staged Fuel Injection," SAE Paper 961163, SAE Transactions, **105**, No. 4, pp. 938-947, 1996.

55. Kanda, T., Hakozaki, T., Uchimoto, T., Hatano, J., Kitayama, N., and Sono, H., "PCCI Operation with Early Injection of Conventional Diesel Fuel," SAE Paper 2005-01-0378, SAE Transactions, **114**, No. 3, pp. 584-593, 2005.

56. Minato, A., Tanaka, T., and Nishimura, T., "Investigation of Premixed Lean Diesel Combustion with Ultra High Pressure Injection," SAE Paper 2005-01-0914, SAE Transactions, **114**, No. 3, pp. 756-764, 2005.

57. Yanagihara, H., Satou, Y., and Mizuta, J., "A Simultaneous Reduction of NOx and Soot in Diesel Engines under a New Combustion System (Uniform Bulky Combustion System - UNIBUS)," 17th International Vienna Motor Symposium, 1996.

58. Hasegawa, R. and Yanagihara, H., "HCCI Combustion in a DI Diesel Engine," SAE Paper 2003-01-0745, SAE Transactions, **112**, No. 3, pp. 1070-1077, 2003.

59. Kimura, S., Aoki, O., Ogawa, H., Muranaka, S., and Enomoto, Y., "New Combustion Concept for Ultra-Clean and High-Efficiency Small DI Diesel Engines," SAE Paper 1999-01-3681, SAE Transactions, **108**, No. 3, pp. 2128-2137, 1999.

60. Kimura, S., Aoki, O., Kitahara, Y., and Aiyoshizawa, E., "Ultra-Clean Combustion Technology Combining a Low-Temperature and Premixed Combustion Concept for Meeting Future Emission Standards," SAE Paper 2001-01-0200, SAE Transactions, **110**, No. 4, pp. 239-248, 2001.

61. Miles, P. C., Choi, D., Pickett, L. M., Singh, I. P., and Henein, N., "Rate-Limiting Processes in Late-Injection, Low-Temperature Diesel Combustion Regimes," Paper presented at Thermo- and Fluid-Dynamic Processes in Diesel Engines: THIESEL 2004, Valencia, Spain, 2004.

62. Kashdan, J. T., Mendez, S., and Bruneaux, G., "On the Origin of Unburned Hydrocarbon Emissions in a Wall-Guided, Low NOx Diesel Combustion System," SAE Paper 2007-01-1836, SAE Transactions, **116**, 2007.

63. Yang, B. and Ghandhi, J., "Measurement of Diesel Spray Impingement and Fuel Film Characteristics Using Refractive Index Matching Method," SAE Paper 2007-01-0485, 2007.

64. Okude, K., Mori, K., Shiino, S., and Moriya, T., "Premixed Compression Ignition (PCI) Combustion for Simultaneous Reduction of NOx and Soot in Diesel Engine," SAE Paper 2004-01-1907, SAE Transactions, **113**, No. 4, pp. 1002-1013, 2004.

65. Parks, J., Partridge, B., and Whitcare, S., "Rapid In Situ Measurement of Fuel Dilution of Oil in a Diesel Engine Using Laser-Induced Fluorescence Spectroscopy," SAE Paper 2007-01-4108, 2007.

66. Singh, S. S., Reitz, R. D., Musculus, M. P., and Lachaux, T., "Validation of Engine Combustion Models Using Detailed In-Cylinder Optical Diagnostics Data for a Heavy-Duty Compression-Ignition Engine," Int.J.Engine Res., **8**, No. 1, pp. 97-126, 2006.

67. Kook, S., Pickett, L. M., Musculus, M. P. B., and Gehmlich, R. K., "Liquid-Phase Diesel Spray Penetration during End-of-Injection Transient," Submitted to Comodia, 2008.

68. Genzale, C. L., Reitz, R. D., and Musculus, M. P. B., "Effects of Piston Bowl Geometry on Mixture Development and Late-Injection Low-Temperature Combustion in a Heavy-Duty Diesel Engine," SAE Paper 2008-01-1330, 2008.

69. Musculus, M. P. B., Lachaux, T., Pickett, L. M., and Idicheria, C. A., "End-of-Injection Over-Mixing and Unburned Hydrocarbon Emissions in Low-Temperature-Combustion Diesel Engines," SAE Paper 2007-01-0907, SAE Transactions, **116**, 2007.

70. Lachaux, T. and Musculus, M. P. B., "In-Cylinder Unburned Hydrocarbon Visualization During Low-Temperature Compression-Ignition Engine Combustion Using Formaldehyde PLIF," Proc.Combust.Inst., **31**, pp. 2921-2929, 2007.

71. Idicheria, C. A. and Pickett, L. M., "Effect of EGR on Diesel Premixed-Burn Equivalence Ratio," Proc.Combust.Inst., **31**, pp. 2931-2938, 2007.

72. Upatnieks, A., Mueller, C. J., and Martin, G. C., "The Influence of Charge-Gas Dilution and Temperature on DI Diesel Combustion Processes Using a Short-Ignition-Delay, Oxygenated Fuel," SAE Paper 2005-01-2088, SAE Transactions, **114**, No. 4, 2005.

73. Pickett, L. M. and Idicheria, C. A., "Soot Formation in Diesel Combustion Under High-EGR Conditions," SAE Paper 2005-01-3834, SAE Transactions, **114**, No. 4, pp. 1559-1574, 2005.

74. Siebers, D., Higgins, B., and Pickett, L., "Flame Lift-Off on Direct-Injection Diesel Fuel Jets: Oxygen Concentration Effects," SAE Paper 2002-01-0890, SAE Transactions, **111**, No. 3, pp. 1490-1509, 2002.

75. Cheng, A. S., Upatnieks, A., and Mueller, C. J., "Investigation of Fuel Effects on Dilute, Mixing-Controlled Combustion in an Optical Direct-Injection Diesel Engine," Energy & Fuels, **21**, No. 4, pp. 1989-2002, 2007.

76. Li, T., Okabe, Y., Izumi, H., Shudo, T., and Ogawa, H., "Dependence of Ultra-High EGR Low Temperature Diesel Combustion on Fuel Properties," SAE Paper 2006-01-3387, 2006.

77. Alriksson, M. and Denbratt, I., "Low Temperature Combustion in a Heavy Duty Diesel Engine Using High Levels of EGR," SAE Paper 2006-01-0075, 2006.

78. Noehre, C., Andersson, M., Johansson, B., and Hultqvist, A., "Characterization of Partially Premixed Combustion," SAE Paper 2006-01-3412, 2006.

79. Colban, W. F., Miles, P. C., and Oh, S., "Effect of Intake Pressure on Emissions from an Automotive Diesel Engine Operating in Low Temperature Combustion Regimes," SAE Paper 2007-01-4063, SAE Transactions, **116**, 2007.

80. Ogawa, H., Miyamoto, N., Shimizu, H., and Kido, S., "Characteristics of Diesel Combustion in Low Oxygen Mixtures with Ultra-High EGR," SAE Paper 2006-01-1147, 2006.

81. Ogawa, H., Li, T., Miyamoto, N., Kido, S., and Shimizu, H., "Dependence of Ultra-High EGR and Low Temperature Diesel Combustion on Fuel Injection

Conditions and Compression Ratio," SAE Paper 2006-01-3386, SAE Transactions, **115**, 2006.

82. Alriksson, M., Gjirja, S., and Denbratt, I., "The Effect of Charge Air and Fuel Injection Parameters on Combustion With High Levels of EGR in a HDDI Single-Cylinder Diesel Engine," SAE Paper 2007-01-0914, 2007.

83. Pickett, L. M. and Idicheria, C. A., "Effects of Ambient Temperature and Density on Soot Formation under High EGR conditions," Paper presented at Thermo- and Fluid-Dynamic Processes in Diesel Engines: THIESEL 2006, Valencia, Spain, 2006.

84. Pickett, L. M., Caton, J. A., Musculus, M. P. B., and Lutz, A. E., "Evaluation of the Equivalence Ratio-Temperature Region of Diesel Soot Precursor Formation Using a Two-Stage Lagrangian Model," Int.J.Engine Res., **7**, pp. 349-370, 2006.